catalysts

MDPI

*Review*

# Recent Development of Single-Atom Catalysis for the Functionalization of Alkenes

**Xuetong Yu [1], Yuxia Ji [1], Yan Jiang [1], Rui Lang [1,2,3,*], Yanxiong Fang [1,2,3] and Botao Qiao [4,*]**

[1] School of Chemical Engineering and Light Industry, Guangdong University of Technology, Guangzhou 510006, China
[2] Guangdong Provincial Key Laboratory of Plant Resources Biorefinery, Guangzhou 510006, China
[3] Jieyang Branch of Chemistry and Chemical Engineering Guangdong Laboratory (Rongjiang Laboratory), Jieyang 515200, China
[4] CAS Key Laboratory of Science and Technology on Applied Catalysis, Dalian Institute of Chemical Physics, Chinese Academy of Sciences, Dalian 116023, China
* Correspondence: langrui@gdut.edu.cn (R.L.); bqiao@dicp.ac.cn (B.Q.)

**Abstract:** The functionalization of alkenes is one of the most important conversions in synthetic chemistry to prepare numerous fine chemicals. Typical procedures, such as hydrosilylation and hydroformylation, are traditionally catalyzed using homogeneous noble metal complexes, while the highly reactive and stable heterogeneous single-atom catalysts (SACs) now provide alternative approaches to fulfill these conversions by combining the advantages of both homogeneous catalysts and heterogeneous nanoparticle catalysts. In this review, the recent achievement in single-atom catalyzed hydrosilylation and hydroformylation reactions are introduced, and we highlight the latest applications of SACs for additive reactions, constructing new C-Y (Y = B, P, S, N) bonds on the terminal carbon atoms of alkenes, and then mention the applications in single-metal-atom catalyzed hydrogenation and epoxidation reactions. We also note that some tandem reactions are conveniently realized in one pot by the concisely fabricated SACs, facilitating the preparation of some pharmaceutical compounds. Lastly, the challenges facing single-atom catalysis for alkene conversions are briefly mentioned.

**Keywords:** single-atom catalysis; alkene; hydrosilylation; hydroformylation; tandem reaction

check for updates

**Citation:** Yu, X.; Ji, Y.; Jiang, Y.; Lang, R.; Fang, Y.; Qiao, B. Recent Development of Single-Atom Catalysis for the Functionalization of Alkenes. *Catalysts* **2023**, *13*, 730. https://doi.org/10.3390/catal13040730

Academic Editors: Leiduan Hao and Jilei Xu

Received: 22 March 2023
Revised: 9 April 2023
Accepted: 11 April 2023
Published: 12 April 2023



## 1. Introduction

The functionalization of alkenes has been a hot topic in synthetic organic chemistry since numerous fine-chemicals, such as silanes [1] and aldehydes [2], can be facilely prepared via versatile alkene intermediates through transition-metal-catalyzed addition reactions on the unsaturated C=C bonds. In this field, some classic homogeneous catalysts, e.g., the Wilkinson's catalyst [2] and the Karstedt's catalyst [3], are widely employed in industrial processes since their high efficiencies could surpass most heterogeneous catalyst analogues with metal nanoparticles (NPs) as active species. However, separating the soluble metal-complex catalysts from reaction residue is quite troublesome; thus, fabricating a kind of highly reactive heterogeneous catalysts is in urgent demand. The main reason for the divergent catalytic reactivity between metal complexes and metal NPs lies in the different dispersion states of active metal species. For the homogenous catalysts dissolved in a reaction solution, nearly all the metal centers are liable to interactions with substrates, whereas only metal species on the outermost surfaces of NPs can play the role of catalytic centers, resulting in low overall reactivity. Therefore, increasing metal utilization efficiencies is indispensable for heterogeneous catalysts to further improve catalytic performances.

Downsizing metal NPs to atomic scales would maximize metal utilization efficiency. However, atomically dispersed metal species are thermodynamically unstable for high surface free energies and thus tend to migrate on support materials and even automatically

integrate as NPs under preparation and/or working conditions. In this respect, suitable support is essential to anchor the isolated metal species. In 2011, Zhang's group found that the $FeO_x$ support can stabilize single Pt atoms as a single-atom catalyst (SAC), achieving good performance in CO oxidation [4]. Moreover, the atomic dispersion of Pt is well-preserved after reaction, demonstrating that the isolated Pt species are the real active centers. From then on, the field of single-atom catalysis has gradually turned into the research frontier of heterogeneous catalysis [5] since numerous SACs are fabricated and applied to various catalytic transformations [6]. SACs can integrate the advantages of both homogeneous catalysts, for example, the maximized metal utilization efficiency, and heterogeneous catalysts, such as stabilization effect and easy recycling, thus providing an ideal solution for the heterogenization of homogeneous catalysts. After decades of efforts, SACs have been successfully employed in the hydrosilylation and hydroformylation reactions with reactivity comparable to the traditional homogeneous catalysts.

In this review, the latest reports regarding single-atom catalysis for the functionalization of alkenes are introduced, and we highlight the development in regulating the electronic properties of metal species through modification of the support substrates. The catalytic mechanisms of hydrosilylation and hydroformylation are proposed. Following this, the effectiveness of SACs in constructing new C-Y (Y = B, P, S and N) bonds on the terminal carbon atoms of alkenes is briefly discussed. Additionally, the hydrogenation and epoxidation reactions are traditionally fulfilled by NP catalysts, while SACs can provide simplified research models for theoretical calculations to investigate reaction mechanisms. It is worth noting that tandem functionalization of alkenes can fulfill multi-steps in one pot, and SACs have been successfully used for this purpose. Finally, we talk about some future opportunities facing single-atom catalysis.

## 2. The Functionalization of Alkenes

### *2.1. Hydrosilylation*

The hydrosilylation reaction is widely utilized in preparing silicone-based materials such as aerogels and surfactants. Among various catalysts, homogeneous Pt catalysts are frequently used in industrial processes. In general, the reaction mechanisms of alkene hydrosilylation over Pt (0) catalysts include the Chalk–Harrod or modified Chalk–Harrod mechanism [7]. As shown in Scheme 1, the Chalk–Harrod mechanism is divided into three steps: (1) Si-H oxidative addition to Pt, (2) alkene insertion into the Pt-H bond, and (3) Si-C reductive elimination. In the modified Chalk–Harrod mechanism, the second step is replaced by alkene insertion into the Pt-Si bond, followed by the C-H reductive elimination. Therefore, a typical Karstedt's catalyst, with the zero oxidation state at the Pt center, could exhibit superior catalytic performance for anti-Markovnikov addition hydrosilylation reactions even under mild working temperatures [3]. However, certain kinds of problems, especially concerning the separation and recycling of homogeneous catalysts, will always persist. Therefore, Pt-based SACs are likely the alternatives to replace traditional Pt-complex catalysts.

In this context, one of the most important issues lies in the fabrication of stable Pt SACs (Figure 1a). In 2017, Beller's group presented the first heterogeneous single-atom Pt catalyst for hydrosilylation reactions [8]. They anchored isolated Pt species on alumina nanorods and thus prepared Pt/NR-$Al_2O_3$-IP with high reactivity comparable to Karstedt's catalyst, demonstrating that SACs can be as effective as homogeneous catalysts. Moreover, various functional groups on the alkenes can be tolerated by Pt/NR-$Al_2O_3$-IP SAC, which can be separated and reused with good stability.

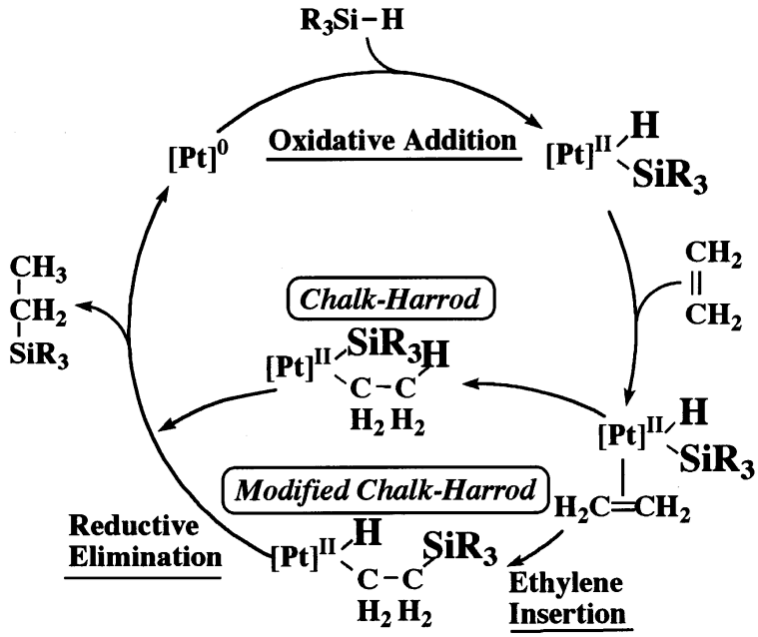


**Scheme 1.** Chalk–Harrod and modified Chalk–Harrod mechanisms of alkene hydrosilylation over Pt-based catalysts. Reproduced with permission from ref. [7] Copyright 1999 Elsevier.

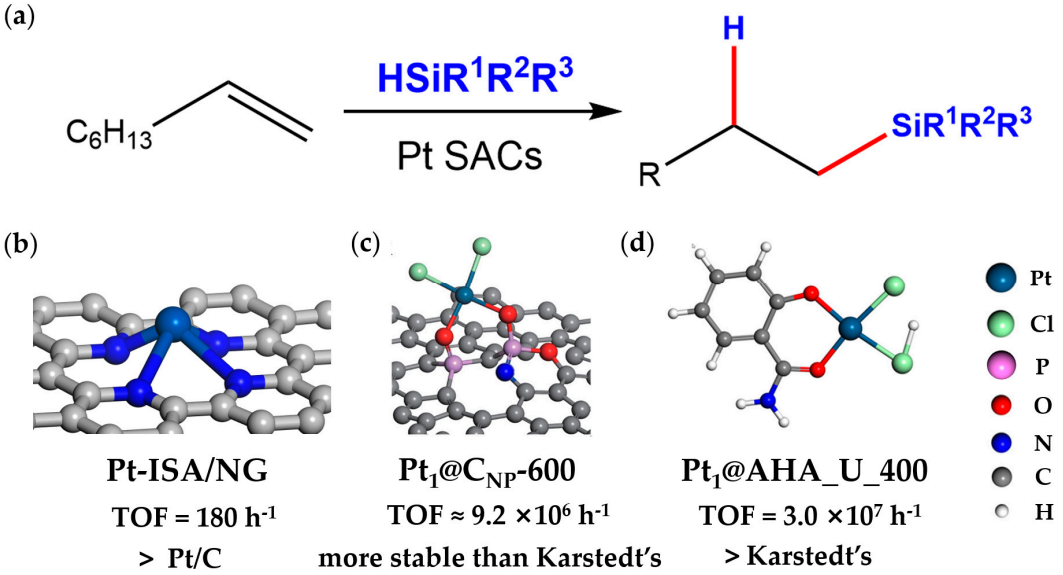


**Figure 1.** (**a**) Representative Pt SACs for hydrosilylation reactions. (**b**–**d**) The structure models of catalytic sites and the corresponding hydrosilylation reactivities of Pt-ISA/NG, $Pt_1$@AHA_U_400, and $Pt_1$@$C_{NP}$-600. Different elements are presented in different colors in the right column. Adapted with permission from ref. [9] Copyright 2018 American Chemical Society, ref. [10] Copyright 2021 John Wiley and Sons, and ref. [11] Copyright 2023 John Wiley and Sons, respectively.

With the first successful case of single Pt atoms catalyzed hydrosilylation in hand, more efforts have been devoted to further improve catalytic performance by regulating the coordination structure of Pt active centers. Carbon-based supports are widely used in industrial processes due to their low cost, high surface areas, and tunable surface properties since the heteroatoms (O, N, P, and S) can be easily doped on/in the carbon materials. Therefore, some carbon-supported Pt SACs are investigated here in detail regarding their potential industrial applications. For example, up to 5.3 wt% loading of Pt is atomically dispersed on the N-doped graphene (Pt-ISA/NG) with the $Na_2CO_3$-assisted one-pot pyrolysis synthetic strategy [9]. In the benchmark reaction of hydrosilylation

of 1-octene, Pt-ISA/NG with a stable Pt-$N_4$ site (Figure 1b) exhibited high selectivity. The reactivity of Pt-ISA/NG was 4 times higher than that of commercial Pt/C with the same Pt loadings, suggesting that the completely exposed metal centers are pivotal for achieving high catalytic performance [9]. In addition, P was added along with N to tune the electronic state of Pt centers with a similar structure. The PN-doped carbon nanofibers were fabricated based on the reaction between $P_2O_5$ and *N*-Methyl-2-pyrrolidone. Pt single-atoms were anchored by the -PN- units on the support (Figure 1c) and denoted as $Pt_1@C_{NP}$-600, which displayed high TOF for hydrosilylation ($9.2 \times 10^6$ $h^{-1}$) and 99% selectivity [10]. Unlike the traditional (modified) Chalk–Harrod mechanism, the reaction mechanism of $Pt_1@C_{NP}$-600 showed the in situ formation of cyclization of ketene oligomers and subsequent polymerization at elevated temperatures, as evidenced by the FTIR and NMR results. Moreover, doping of O and Cl with Pt atoms resulted in electron-deficient Pt centers. For example, Pt SAC supported on humic matter ($Pt_1$@AHA_U_400) showed the best activity thus far in hydrosilylation of 1-octene (TOF = $3.0 \times 10^7$ $h^{-1}$) with >99% selectivity [11]. DFT calculations revealed that this high performance can be attributed to the atomic dispersion and the electron-deficiency state of Pt species since Pt was connected with two Cl and two O ions (Figure 1d). According to DFT calculations, $Pt_1$@AHA_U_400 prefers to undergo the modified Chalk–Harrod mechanism regarding hydrosilylation reactions, owing to its low energy barrier.

Besides heteroatom doping, the carbon support could also offer a versatile platform to add another metal species alloying with Pt. In this case, Fe was added to form a $PtFe_3$ catalytic center on N-doped carbon spheres ($PtFe_3$/CN) [12]. The electrons could transfer from neighboring Fe species to Pt single atoms in a $PtFe_3$/CN catalyst. Consequently, the electron-rich isolated $PtFe_3$ sites showed higher catalytic performance (99% selectivity and ca. 740,000 of TON) than the $Pt_1$/CN SAC and $K_2PtCl_6$ homogeneous catalysts. The hydrosilylation mechanism of the $PtFe_3$/CN catalyst was investigated using DFT calculations, proposing the Chalk–Harrod mechanism: Si-H bond oxidative addition to isolated Pt center and alkene insertion into the Pt-H bond. These results show that the electron-rich catalytic centers may further improve the hydrosilylation reactivity; however, these sites may be more vulnerable to aggregate than the electron-deficient Pt sites. Therefore, a porous confinement strategy is developed to locate the Pt sites within a nanocage and maintain the valance of Pt between 0 and +2. The confined Pt SAC (COP1-T-Pt) was ten times more active than the Karstedt's catalyst [13]. Besides, remarkable site-selectivity as well as good recyclability of COP1-T-Pt was achieved. Both quantitative EXAFS fitting and FDMNES simulation supported that Pt was anchored by the surrounding Pt-C and Pt-Si bonds, forming a familiar structure as the key intermediate in the Chalk–Harrod mechanism.

The above cases illustrate that isolated Pt centers may be suitable replacements for the conventional homogeneous catalysts in hydrosilylation reactions. Inspired by these results, other noble metals have also been employed. A recent example showed that $ZrO_2$-supported Ru SAC was more reactive than the $RuCl_3$ homogeneous catalyst in ethylene hydrosilylation [14]. The reaction mechanism on the $Ru^{\delta+}/ZrO_2$ SAC is proposed to follow the Chalk–Harrod mechanism according to DFT simulation. Based on the mechanism insights obtained from Pt-based SACs, we can anticipate that the electronic state of other metal species may be further tuned by the coordinating species, such as heteroatoms, to achieve better catalytic performance than homogeneous catalysts.

### *2.2. Hydroformylation*

Currently, the hydroformylation reaction is homogeneously catalyzed in industrial processes, producing aldehydes from olefins and syngas ($CO/H_2$). Compared to the above hydrosilylation reaction, achieving high chemo-selectivity in hydroformylation reactions is quite difficult as the side-reaction of olefin hydrogenation simultaneously occurs under $H_2$ atmospheres. Consequently, the homogeneous Wilkinson's catalyst ($RhCl(PPh_3)_3$) is frequently used for its high reactivity and chemo-selectivity, while in the heterogenous catalysts, compared with Rh NPs, the singly dispersed Rh species are more capable to

prevent hydrogenation pathways due to the relatively weak bonding effect with $H_2$ [15]. However, isolated metal ions may be reduced with CO and/or $H_2$ gas, resulting in the deactivation of catalysts via aggregation. Therefore, the active structure of SACs should achieve a balance between strong stabilization effects to prevent sintering and flexible coordination with substrates [16].

Regarding oxide supports, three synthetic strategies are developed to design stable and reactive Rh SACs, including creating oxygen vacancies on the supports (Figure 2a), fabricating dual-metal sites (Figure 2b), and forming metal alloy species (Figure 2c). A systematic study on some representative oxide-supported Rh SACs was performed, correlating the densities of oxygen vacancies with catalytic performances (Figure 2a) [17]. It is obvious that the existence of oxygen vacancies on the oxide surface leads to the dominant hydroformylation pathway rather than the hydrogenation reaction. Moreover, the oxygen-defective $SnO_2$-supported Rh SAC showed hundreds of times higher reactivity than that on $ZrO_2$ support in the gas-phase hydroformylation of ethylene. These results revealed that the delicate design of the surface defects, such as vacancies and step sites, are helpful for achieving excellent catalytic activity on the reducible-oxide-supported Rh SACs. As shown in Scheme 2, the Heck–Breslow mechanism is proposed for the Rh catalysts on the oxygen-defective support. After CO and H adsorption, insertion of ethylene into the Rh-H bond provided an ethyl group. Following this, an additional CO molecule inserted into the Rh-ethyl bond, and the subsequent reductive elimination formed the final product. However, oxygen vacancies are rarely found on inert oxides such as $Al_2O_3$ and $SiO_2$, so dual metal sites are concisely fabricated to increase reactivity. In the case of $Al_2O_3$-supported Rh-$WO_x$ catalysts (Figure 2b), increasing the loading of $WO_x$ could lead to different structures of catalytic sites, and the atomically dispersed Rh-W pair sites achieved the highest rate of ethylene hydroformylation to propanal [18]. Unlike traditional Rh SACs, the synergetic effects of Rh and W species was suggested by unique mechanism calculations involving Rh-assisted $WO_x$ reduction, ethylene transfer from $WO_x$ to Rh atoms, and $H_2$ dissociation at the Rh-$WO_x$ interface (Scheme 3). In the above two cases, the Rh centers are both in the positive valence state, while the electron-rich Rh single atoms are seldom reported. We fabricated ZnO-nanowire-supported Rh SACs and used the in situ EXANES and XPS techniques to verify that after mild $H_2$ reduction at 200 °C, the isolated Rh species were at the approximately $Rh^0$ state (Figure 2c) [19]. A plausible explanation for this is that $Zn^{2+}$ was simultaneously reduced to $Zn^0$, transforming electrons to lower the oxidation state of the nearby Rh species. The Rh/ZnO SACs were even slightly more reactive and chemo-selective than the homogeneous Wilkinson's catalyst in styrene hydroformylation (Figure 2c), demonstrating that regulating the valence state of Rh sites is pivotal for achieving excellent catalytic performance.

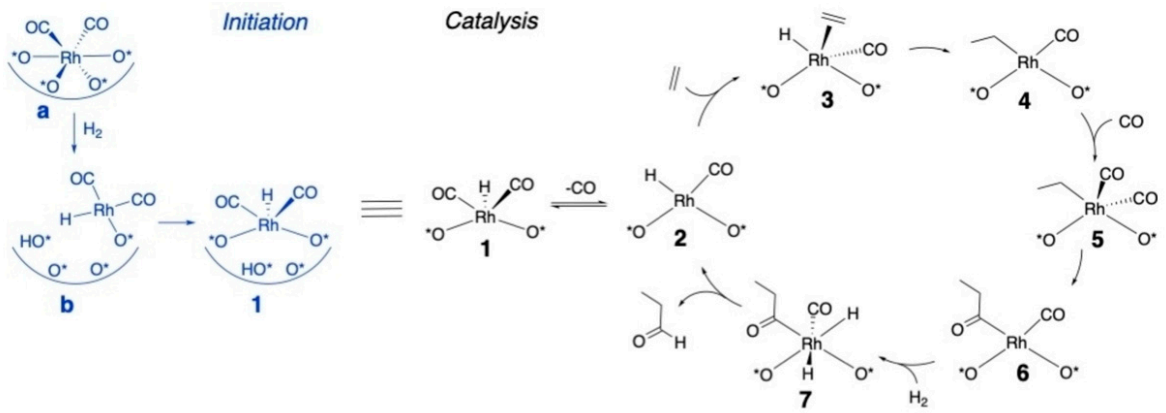


**Scheme 2.** The Heck–Breslow mechanism of hydroformylation. O* represents the lattice O. Reproduced with permission from ref. [17] Copyright 2022 John Wiley and Sons.

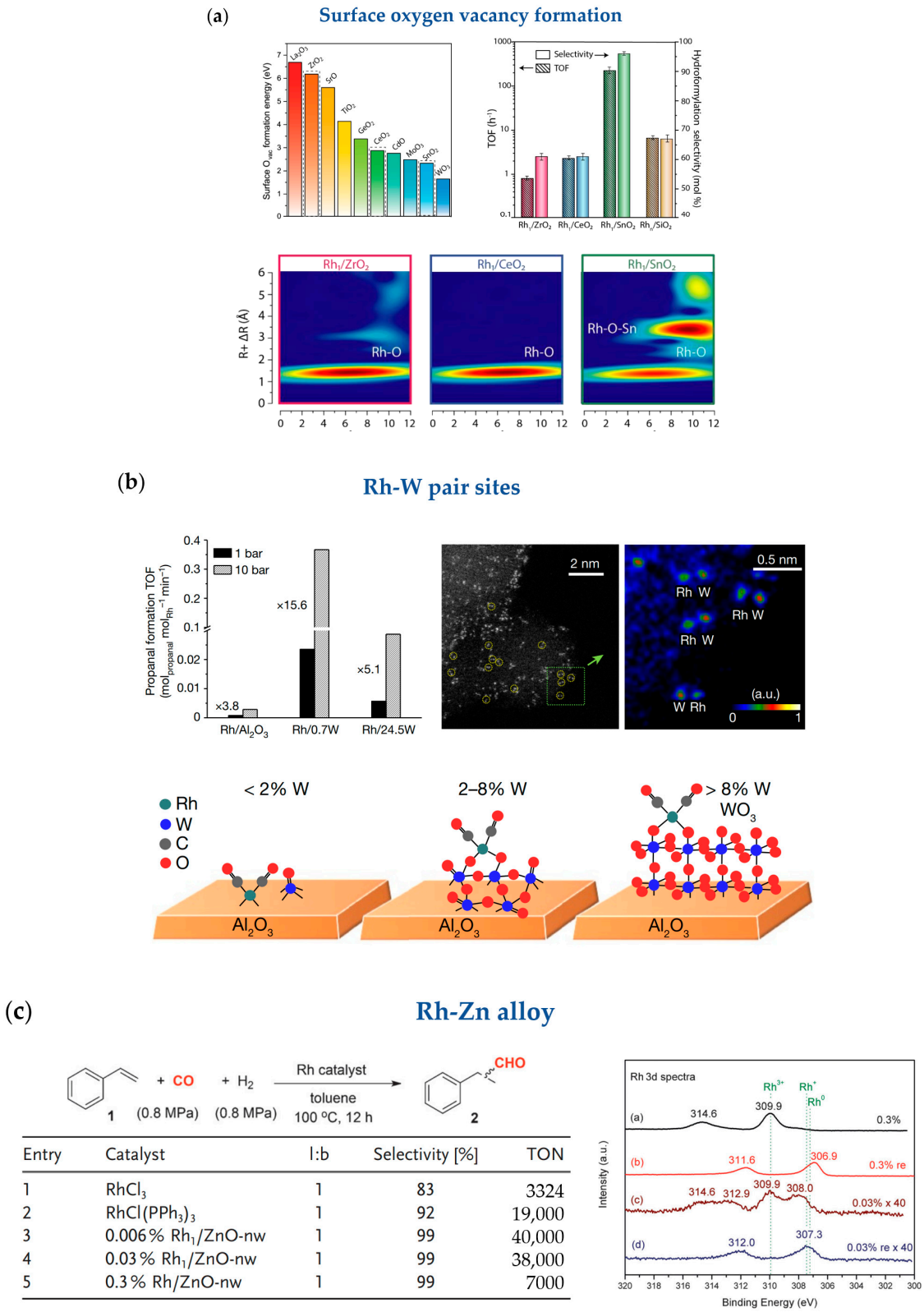


| Entry | Catalyst | l:b | Selectivity [%] | TON |
|---|---|---|---|---|
| 1 | $RhCl_3$ | 1 | 83 | 3324 |
| 2 | $RhCl(PPh_3)_3$ | 1 | 92 | 19,000 |
| 3 | 0.006 % $Rh_1$/ZnO-nw | 1 | 99 | 40,000 |
| 4 | 0.03 % $Rh_1$/ZnO-nw | 1 | 99 | 38,000 |
| 5 | 0.3 % Rh/ZnO-nw | 1 | 99 | 7000 |

**Figure 2.** Three strategies to improve the hydroformylation reactivity of oxide-supported Rh SACs. (**a**) Creating surface oxygen vacancies on the oxide support, (**b**) constructing the Rh-W pair sites, and (**c**) forming a Rh-Zn alloy. Reproduced with permission from ref. [17] Copyright 2022 John Wiley and Sons, ref. [18] Copyright 2022 Springer Nature, and ref. [19] Copyright 2016 John Wiley and Sons.

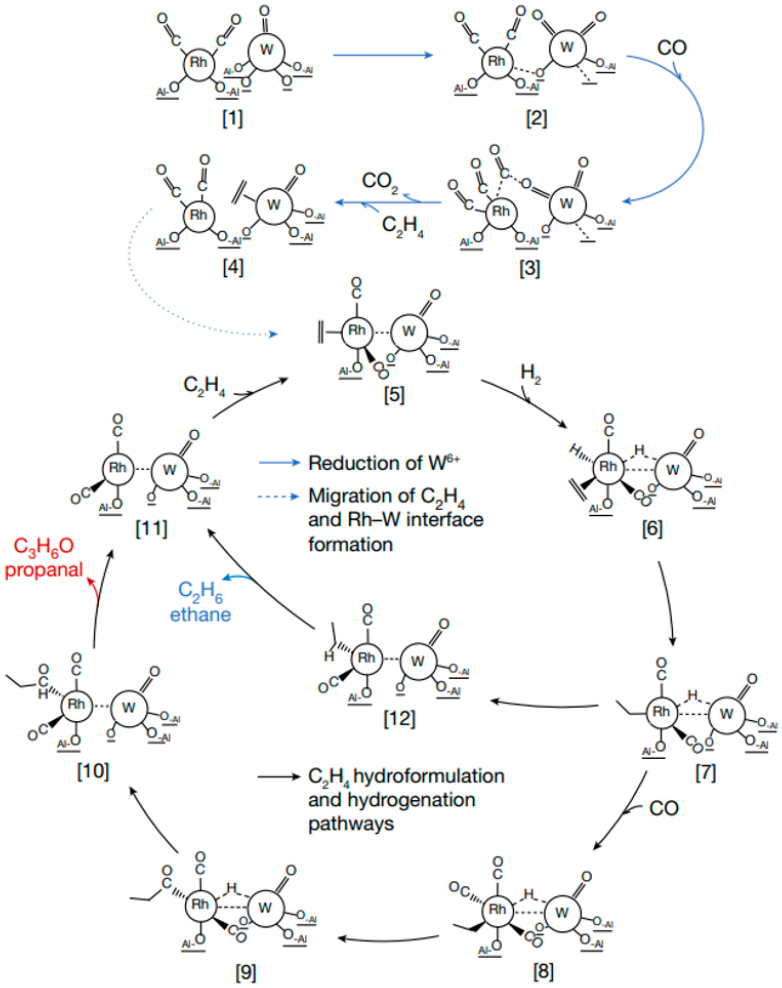


**Scheme 3.** Hydroformylation mechanism at the Rh-$WO_x$ interface. Reproduced with permission from ref. [18] Copyright 2022 Springer Nature.

Although very high reactivity is fulfilled by the oxide-supported Rh SACs, regio-selectivity in hydroformylation is another concern. For the SACs on the open oxide supports, a similar number of linear and branched aldehyde products always generate at the same time [19]. Therefore, the spatial confinement strategy is thus developed to precisely control the regioselectivity. In this context, the zeolite matrix [20] and the porous polymer [21] are identified as suitable supports to locate single Rh atoms. The Rh@Y zeolite catalyst was prepared with the in situ hydrothermal method, achieving 100% chemo-selectivity and good regioselectivity toward heptanal (linear/branched = 2.2) in the hydroformylation reaction of 1-hexene [20]. Inspired by the homogeneous catalytic systems, wherein high regio-selectivity can be obtained by adding excess amount of phosphine ligands, Rh@POP-PTBA-HA-50 was designed to encapsulate atomically dispersed Rh species within porous monophosphine polymers (Figure 3), and the selectivity of linear aldehyde was remarkably increased to 92% in 1-octene hydroformylation [21]. Detailed mechanism studies revealed that abundant phosphine ligands within polymer substrates endow the isolated Rh sites with high activity and stability. The similar coordinating effect of N to the single metal centers might also promote regioselectivity. For example, a Ru@NC SAC exhibited very good activity (TOF = 12,000 $h^{-1}$) and remarkable regioselectivity (linear/branched = 93:7) in the hydroformylation of 1-hexene, owing to the presence of Ru(II)-$N_x$-active species on the N-doped carbon support [22].

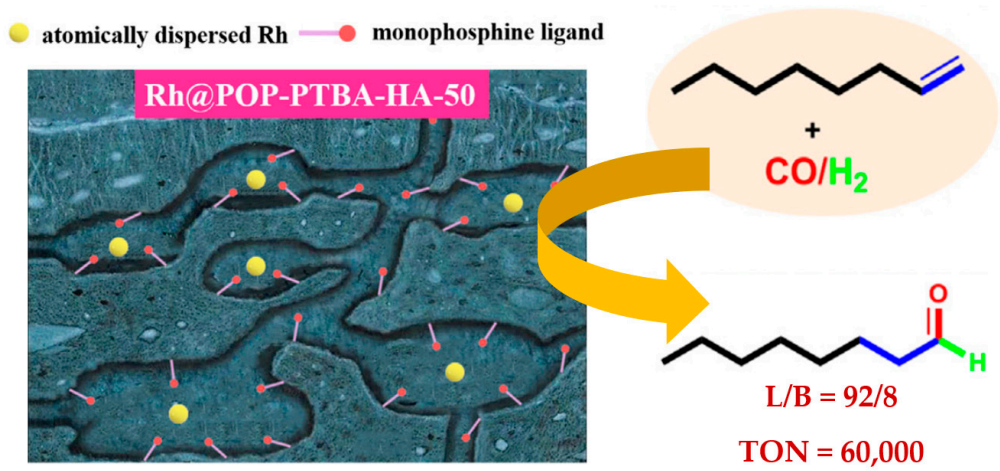


**Figure 3.** The confinement of a porous structure can improve regioselectivity in hydroformylation. Adapted with permission from ref. [21] Copyright 2021 Elsevier.

The heteroatom-doped strategy can even be applied to the non-noble metal SACs on oxide materials. The ZrP-supported Co SAC showed 91.3% aldehyde selectivity in 1-octene hydroformylation [23]. The strong bonding effect between Co sites and the phosphate groups on ZrP are the origins responsible for suppression of Co ions regarding leaching, thus improving the catalytic performance and stability of the Co SAC. In situ FT-IR analysis was used to clarify the reaction mechanism. As shown in Scheme 4, the proposed reaction pathway involved the following steps such as alkene coordination, hydride and CO migratory insertion forming the acyl-like species, and reductive elimination. Currently, Co-based SACs attract much attention as next-generation hydroformylation catalysts, since the reactivity of Co SAC is very similar to that of Rh catalysts, as evidenced by the case of $Co_1/\beta$-$Mo_2C$ in the hydroformylation of propene [24].

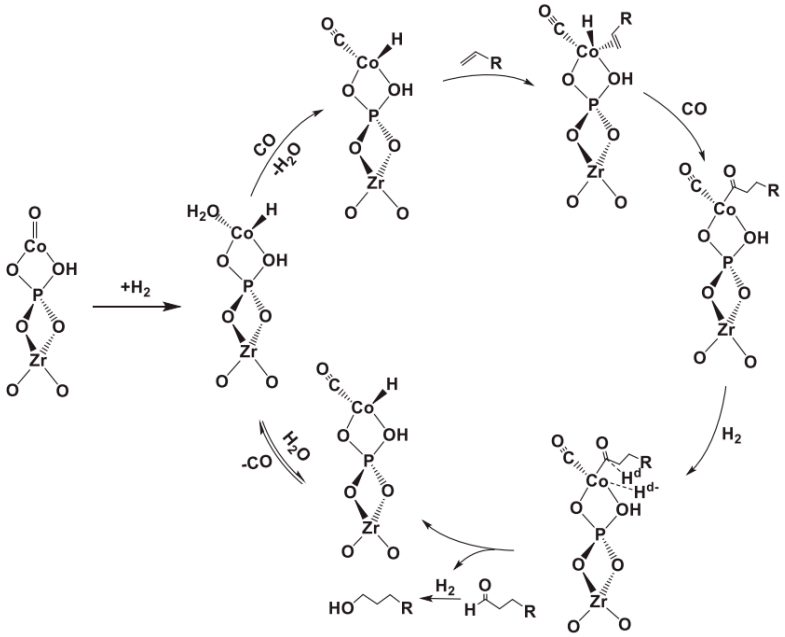


**Scheme 4.** Proposed hydroformylation mechanism involving a CoZrP-2.0 catalyst. Reproduced with permission from ref. [23] Copyright 2022 Elsevier.

### *2.3. Constructing C-Y (Y = B, P, S, N) Bonds*

Besides the above C-Si and C-C bonds forming, SACs have also been used in constructing some interesting C-Y (Y = B, P, S, N) bonds through hydroboration, hydrophosphinylation, sulfonation, and aziridination of olefins, respectively. The regioselective hydroboration of alkenes is a direct method to synthesize linear alkylboronic esters. In this reaction, the isolated Pt species are frequently used as active sites, and the catalytic activities are dramatically influenced by the coordination environment of Pt centers. For example, three different coordination structures of single-atom Pt species, denoted as SA Pt-$O_3$, SA Pt-$O_2$, and SA Pt-$N_4$, respectively, have been thoroughly investigated in the anti-Markovnikov hydroboration of 1-octene, and SA Pt-$O_3$ (Figure 4a) exhibited the highest activity (TON = 3288) along with good selectivity (97%) [25]. DFT calculations suggested that the unique coordination structure of three O species with Pt could decrease the active energy. Two possible pathways of alkene hydroboration for SA Pt-$O_3$ were shown in Figure 4b, while the mechanism involving the hydroboration of $C_8H_{17}$* (blue line) was more favorable.

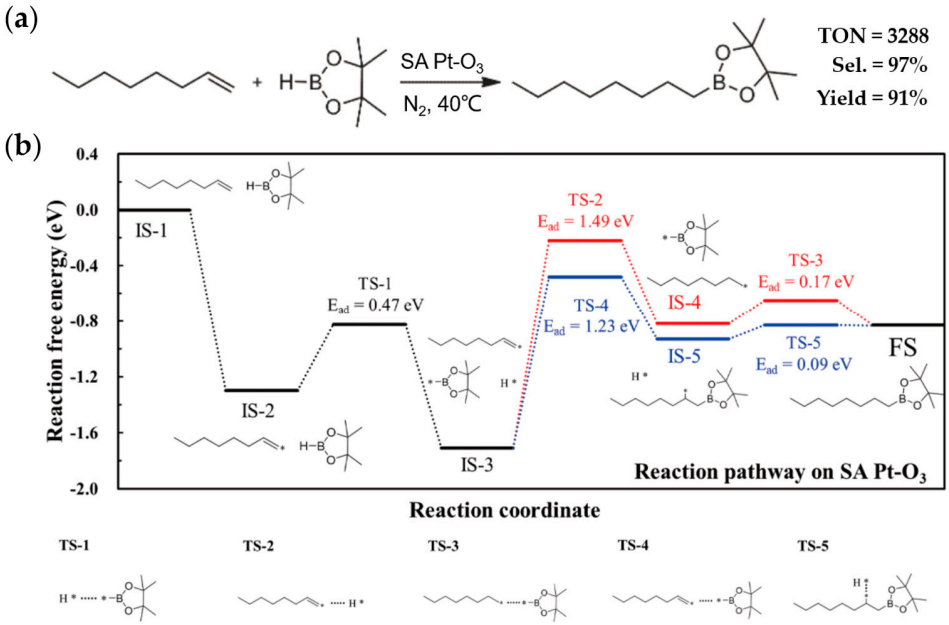


**Figure 4.** (**a**) Hydroboration of 1-octene over SA Pt-$O_3$. (**b**) Two different reaction pathways of alkene hydroboration over SA Pt-$O_3$. Both adapted with permission from ref. [25] Copyright 2020 Springer Nature.

The hydrophosphinylation of alkenes is regarded as a convenient method to produce valuable alkylphosphorus compounds. However, low catalytic efficiency was the main obstacle for homogeneous catalysts, probably caused by the strong poisoning effect of P with metal centers, while heterogeneous catalysts stabilizing on the solid supports may overcome this issue with the aid of strong metal–support interactions. As shown in Figure 5a, a Cu SAC on $Al^{3+}$-doped MgO nanosheets ($Cu_1$/MgO(Al)) showed 99% selectivity and high durability in the anti-Markovnikov hydrophosphinylation of various alkenes [26]. Moreover, single Cu atoms accelerated the initiating step of forming phosphinoyl radicals, achieving high TOF (1272 $h^{-1}$), which was even better than that of traditional homogeneous catalyst. According to the DFT study, the free-radical mechanism was proposed (Figure 5b, black line).

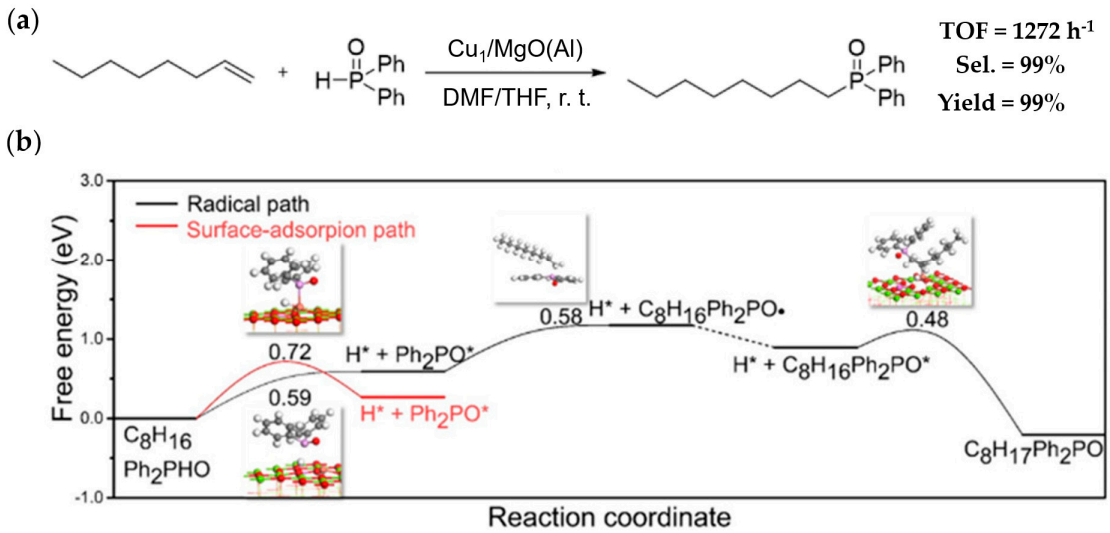


**Figure 5.** (**a**) hydrophosphinylation of 1-octene over $Cu_1$/MgO(Al); (**b**) Free energy diagram for the hydrophosphinylation over $Cu_1$/MgO(Al). Both adapted with permission from ref. [26] Copyright 2022 American Chemical Society.

Carbon nitride (CN) and $TiO_2$ are frequently used in photocatalysis as support materials for the capability to separate photogenerated electron pairs and holes. Recently, single-atom photocatalysts have been attracting increasing attention because of their improved photocatalytic performance. As shown in Figure 6a, Wen and co-workers reported a biomimetic single Fe-atom photocatalyst CNH through coupling CN with hemin [27]. Under visible light irradiation, up to 94% yield of $\beta$-ketosulfone was obtained with the CNH-catalyzed sulfonation reaction. Later, the same group prepared another SAC, Ni/$TiO_2$, which can be easily scaled up for photocatalytic site-selective sulfonation, transforming enamide to $\alpha$-amidosulfones and $\beta$-propionamidosulfones with TON levels as high as 18,963 under visible light (Figure 6b) [28].

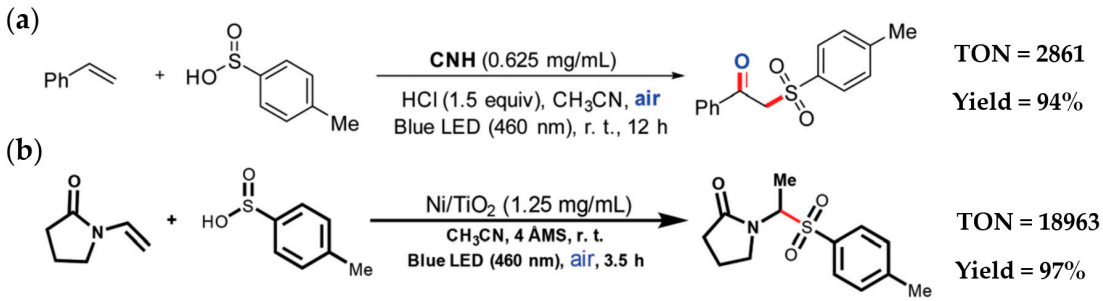


**Figure 6.** (**a**) Sulfonation reaction on CNH to obtain $\beta$-ketosulfone. (**b**) Sulfonation reaction on Ni/$TiO_2$ to obtain $\alpha$-amidosulfones. Reproduced with permission from ref. [27] Copyright 2020 Royal Society of Chemistry and ref. [28] Copyright 2022 Royal Society of Chemistry.

Recently, an unprecedented C-N bond formation of alkenes was revealed by a Co SAC, namely $Co_{SA}$-N/C, which was derived from a bimetal-organic framework. $Co_{SA}$-N/C showed good aziridination activity, transforming alkene to aziridine at 0 °C (Figure 7a) and further achieved direct oxyamination (Figure 7b) by adding methanol into the reaction system. The substrate scope can expand to a series of styrene derivatives and dienes, and some drug-derived olefins could also smoothly undergo the aziridination process [29]. Based on previous reports and experimental results, the authors proposed a stepwise mechanism shown in Figure 7c.

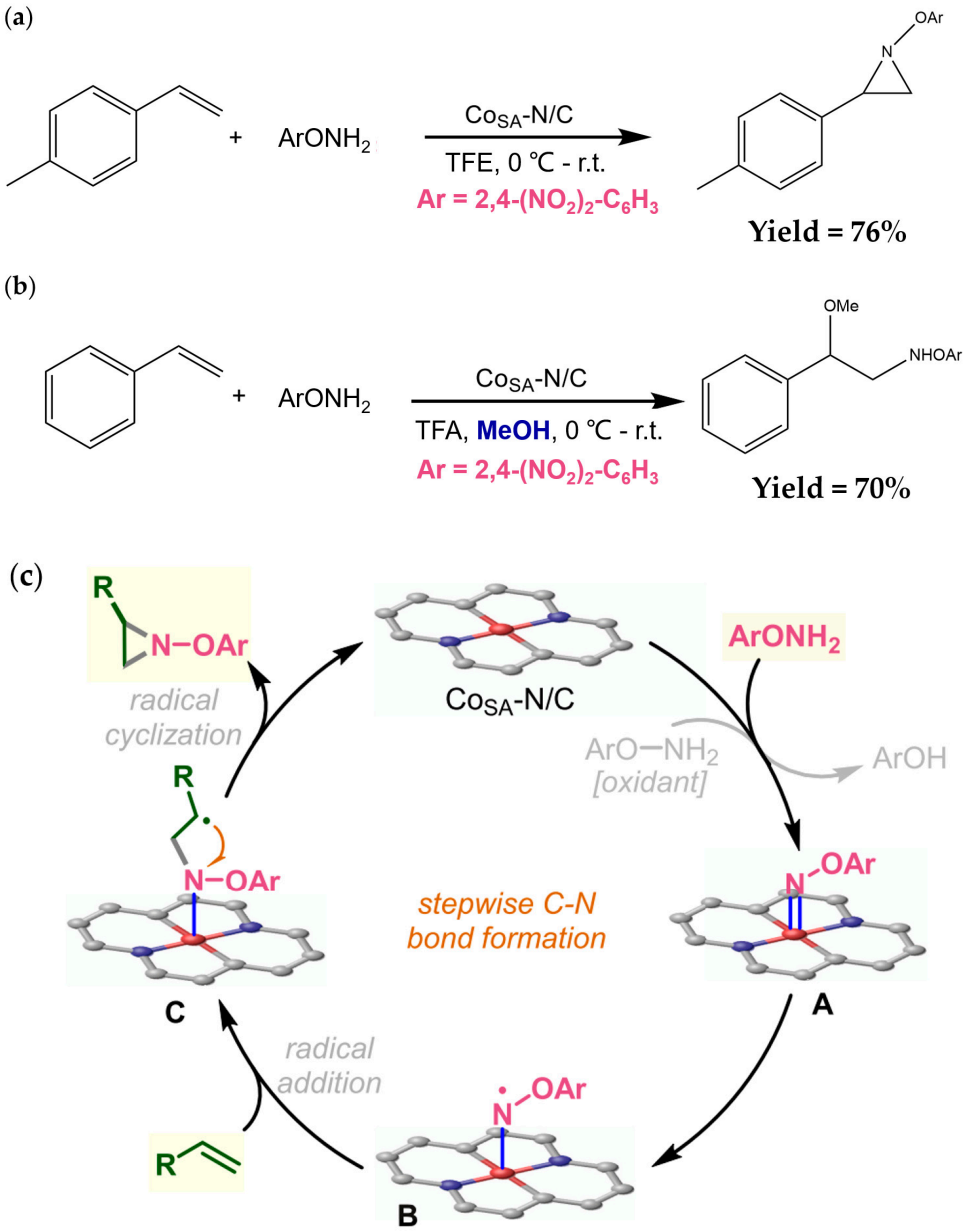


**Figure 7.** Two types of isolated Co-catalyzed C-N coupling reactions under modified working conditions. (**a**) Aziridination of *p*-methylstyrene. (**b**) Oxyamination of styrene. (**c**) Proposed Mechanism of aziridination. All adapted with permission from ref. [29] Copyright 2023 American Chemical Society.

### *2.4. Hydrogenation*

Hydrogenation represents a powerful method to convert alkenes to alkanes, generating a wide range of synthetic intermediates [30]. The single-metal-atom-catalyzed hydrogenation reactions have been previously summarized by many groups [31–35], so in this short review, we only focus on the recent development regarding selectively transforming butadiene to butene as an example, since single Pd/Pt atom-catalyzed selective hydrogenation of 1,3-butadiene plays a crucial role in the purification of dienes in the petrochemical industry, while NP analogues favor the complete hydrogenation process instead [36]. Carbon-based materials are frequently used for their good thermal stability in the hydrogenation reaction [37]. Graphene-supported Pd SAC showed excellent durability against sintering and coking for the 100 h duration and maintained ~70% 1-butene selectivity at 95% conversion, surpassing the Pd-NP catalysts (Figure 8a) [38]. Moreover, $C_3N_4$ can also be used as a photocatalyst, and thus protons can be in situ generated through

photo splitting of water. For example, carbon-nitride-supported Pd SAC ($Pd_1$-mpg-$C_3N_4$) performed the hydrogenation reaction under visible-light irradiation using water as a sustainable source of hydrogen [39]. Besides Pt and Pd, an Ir SAC supported on the nitrogen-rich carbon substrate exhibited high activity to the hydrogenation of butadiene with perfect selectivity (~100%) to butenes even at 200 °C while the selectivity on Ir-NC gradually dropped to ~0% with increasing temperatures (Figure 8b). The operando XAS demonstrated that Ir-$X_3$ (X = C/N/O) was an active site with great stability under working conditions [40].

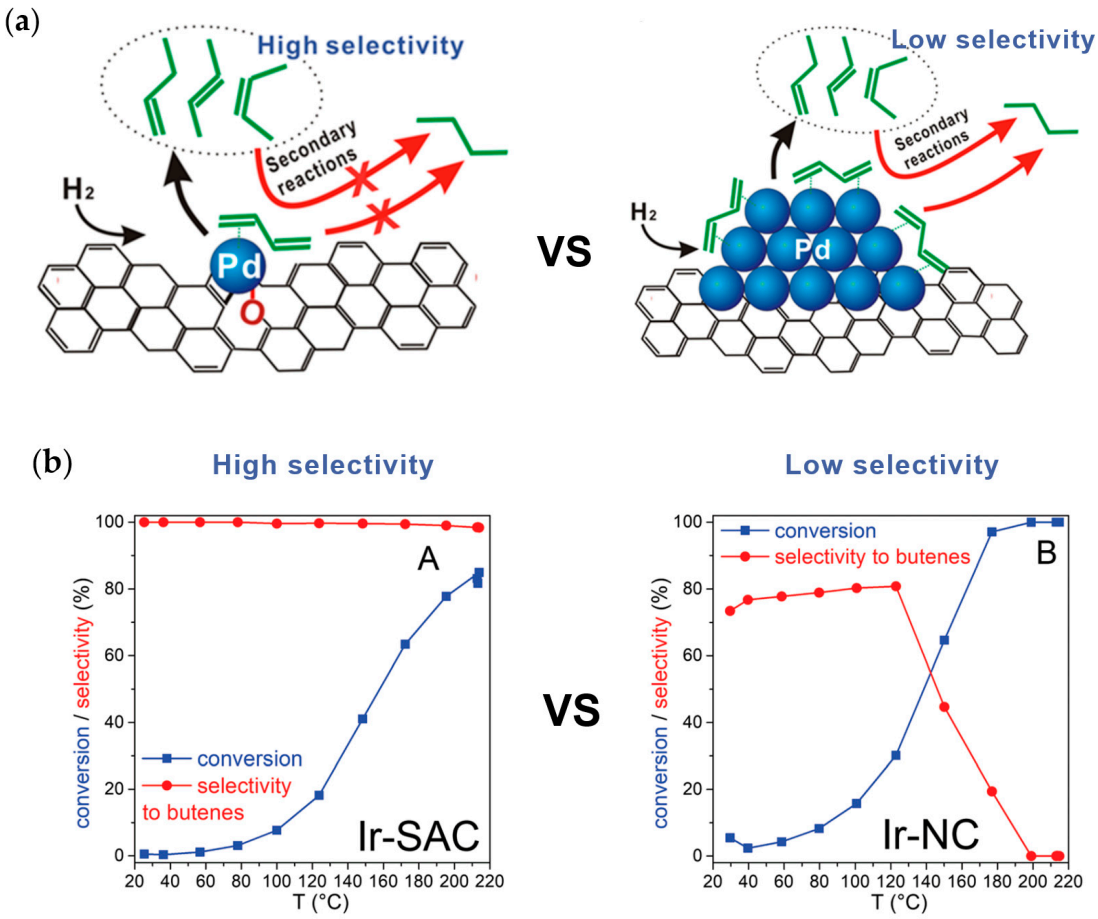


**Figure 8.** (**a**) Schematic illustration of improvement in butene selectivity on single-atom $Pd_1$/graphene catalyst. (**b**) Ir SAC showed the better selectivity at high temperatures. Adapted with permission from ref. [38] Copyright 2015 American Chemical Society and ref. [40] Copyright 2022 Royal Society of Chemistry.

The oxide-supported single-atom alloy (SAA) is also capable of performing conversions with good selectivity. Lucci et al. fabricated the $\gamma$-alumina-supported Pt-Cu SAA with isolated Pt atoms located in the Cu(111) surface. The as-prepared Pt/Cu(111) SAA could display high selectivity and excellent stability under working conditions (Figure 9) [41]. DFT calculations revealed that $H_2$ was readily activated on the single Pt atoms, and the dissociated H species could migrate to the Cu sites through the spillover effect. The selective hydrogenation to butene was attributed to the weak binding of the butadiene substrate on the Cu site.

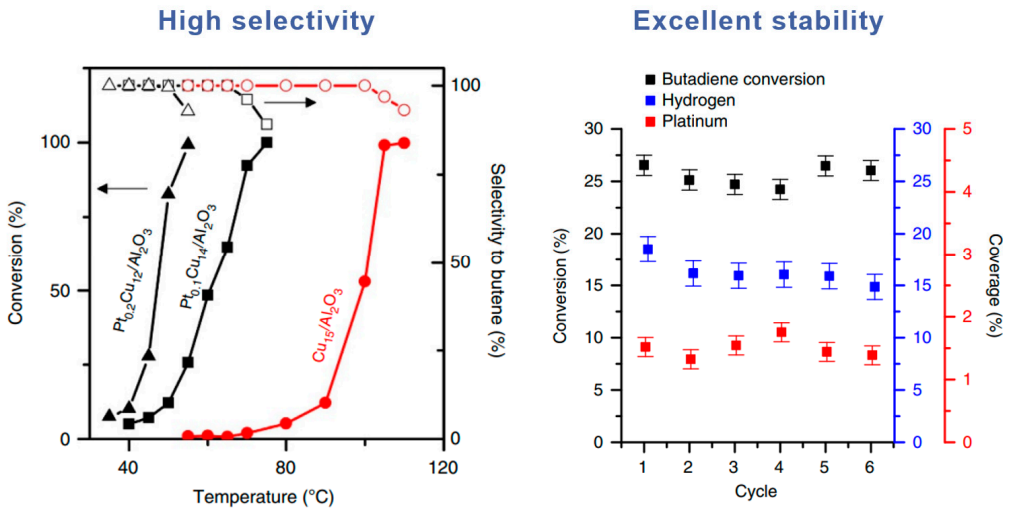


**Figure 9.** The high selectivity and excellent stability displayed by Pt/Cu(111) SAA. Adapted with permission from ref. [41] Copyright 2015 Lucci, F.R. et al.

### *2.5. Epoxidation*

SACs can provide simplified models of catalytic centers, and DFT calculations have thus been frequently used to predict catalytic feasibility. Especially for some reactions utilizing explosive substrates, taking the epoxidation reaction as an example, the computational screening of catalysts is of great help in facilitating the traditional optimizing process, since the most-efficient catalyst can be conveniently selected from the catalyst library without performing many reactions.

The electronic structures of single-metal atoms supported on a phosphotungstic acid (PTA) cluster were systematically investigated with DFT calculations to predict the catalytic performance in ethylene epoxidation. Among the non-noble transition metals (Fe, Co, Ni, etc.), Fe preferred to anchor at the four hollow (4H) site of the PTA cluster [42]. Moreover, the strong covalent metal-support interaction between Fe and PTA is the foundation for high stability. Similarly, according to the literature [43–45], a mechanism for selective oxidation of styrene is proposed in Figure 10a. DFT calculations predicted that the activity of Co-$N_3$ SAC in styrene epoxidation could be further improved by constructing unsaturated defect sites, which underwent lower free energy compared to the Fe-$N_4$, Cu-$N_4$ and Co-$N_4$ structures (Figure 10b) [46]. Using *tert*-butyl hydroperoxide (TBHP) as the oxidant, 99.9% of the styrene conversion was achieved with 71% selectivity to styrene oxide.

In oxidation reactions, $O_2$ is an environmental benign replacement to organic peroxides such as TBHP. Therefore, Chen et al. constructed a vacancy-rich $Co_1$/NC-h SAC from a CoZn-ZIF precursor, aiming to use $O_2$ as the oxygen source. The Co-$N_x$ active site showed high intrinsic activity in the epoxidation of cyclooctene at 140 °C, and the yield of the target product (1,2-epoxycycloheptane) reached 95% [47]. Moreover, the oxide materials are also capable of introducing a large number of vacancies in SACs [48]. For example, Bi vacancies in $Ru_1/Bi_{2-x}WO_6$ SACs can confine Ru species at an atomic scale and provide exceptional efficiency in the epoxidation of trans-stilbene to trans-stilbene oxide [49]. In addition, $Ir_1/\alpha$-$MnO_2$ displayed a remarkable ~99% selectivity in ethylene epoxidation [50]. In situ experiments and quantum-chemistry calculations indicated that the $\pi$-coordination structure between isolated Ir sites and substrates, such as ethylene, and molecular oxygen, can promote the formation of five-membered oxametallacycle intermediates and then accelerate the formation of ethylene oxide. Electrocatalysis is also applied in epoxidation, since Ir-$MnO_x$ SAC exhibited a Faradaic efficiency of 46 ± 4% in cyclooctene epoxidation. Operando XAS characterizations suggested that the electron-deficient Ir sites induced the formation of highly electrophilic oxygen atoms, leading to the enhancement of electrocatalytic performance [51].

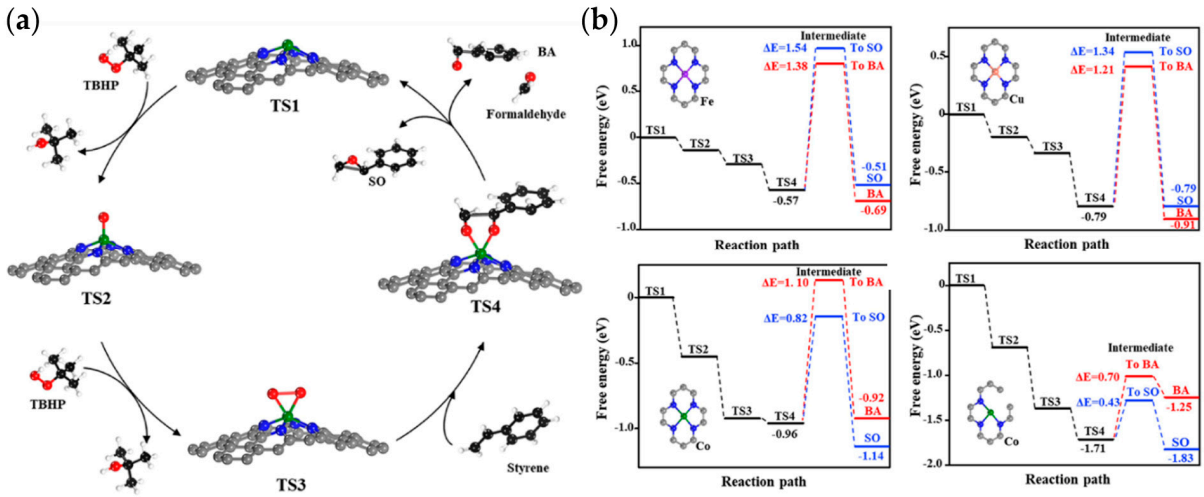


**Figure 10.** (**a**) Mechanism for styrene epoxidation. (**b**) Free energy diagrams for styrene epoxidation on Fe-$N_4$, Cu-$N_4$, Co-$N_4$, and Co-$N_3$ along the reaction pathway. Adapted with permission from ref. [46] Copyright 2022 American Chemical Society.

## 3. Tandem Reactions

Tandem reactions perform two or more catalytic processes successively in one pot. For example, Rh single-atom sites are active in both hydroformylation and hydrogenation reactions, capable of directly transforming alkenes to amines for pharmaceutical synthesis. In this context, fendiline, an anti-anginal agent for the treatment of coronary heart disease, was prepared from easily available substrates, including arylethylene, phenylethylamine, and syngas, via the single Rh atoms catalyzed tandem hydroformylation/reductive amination reactions in 87% overall yield (Figure 11a) [52]. The key to protecting Rh atoms from sintering probably lies in the unique Rh-P coordinating effect and the good stability of nanodiamond support. A similar approach was realized with the $Rh_1$/P25 SAC (Figure 11b), which showed higher selectivity than $[Rh(cod)_2]BF_4$ in hydroaminoalkylation [53]. In situ characterizations suggested that the Rh atoms were singly dispersed on the surface of $TiO_2$, and each Rh species was coordinated with four O atoms on average, fabricating the stable reactive center under working conditions. Additionally, Rh is highly active in the water–gas shift (WGS) reaction, producing $H_2$ from CO and water. Li et al. coupled hydroformylation with WGS reactions and found that the in situ generated $H_2$ is key to the regioselective formation of linear aldehydes (Figure 11c) [54]. Therefore, the linear/branched product ratio reached 3.0 on $Rh_1/CeO_2$ SAC without any addition of phosphine ligands. By contrast, the Rh NP catalyst could also produce $H_2$ from the WGS reaction, but the hydrogenation of aldehyde would occur at the same time, forming undesired alcohol products.

Furthermore, two active metal sites can be combined as tandem catalysts. Sarma et al. reported an olefin isomerization-hydrosilylation reaction by adding two SACs, $Ru_1/CeO_2$ and $Rh_1/CeO_2$, in one pot, achieving 95% regioselectivity to the terminal organosilane [55]. In 2021, a biomimetic SAC ($Pd_1$@$Fe_1$) was fabricated, integrating two kinds of single-metal atoms in the MOF-derived yolk and N-doped carbon shell structure, respectively (Figure 12a) [56]. The single Fe and Pd sites could respectively catalyze nitrobenzene hydrogenation and styrene epoxidation, leading to a cascade synthesis of amino alcohols (Figure 12b). The detailed reaction mechanism was investigated by the control experiments (Figure 12c) and DFT calculations (Figure 12d), providing a versatile strategy to integrate different kinds of SACs within one reaction system.

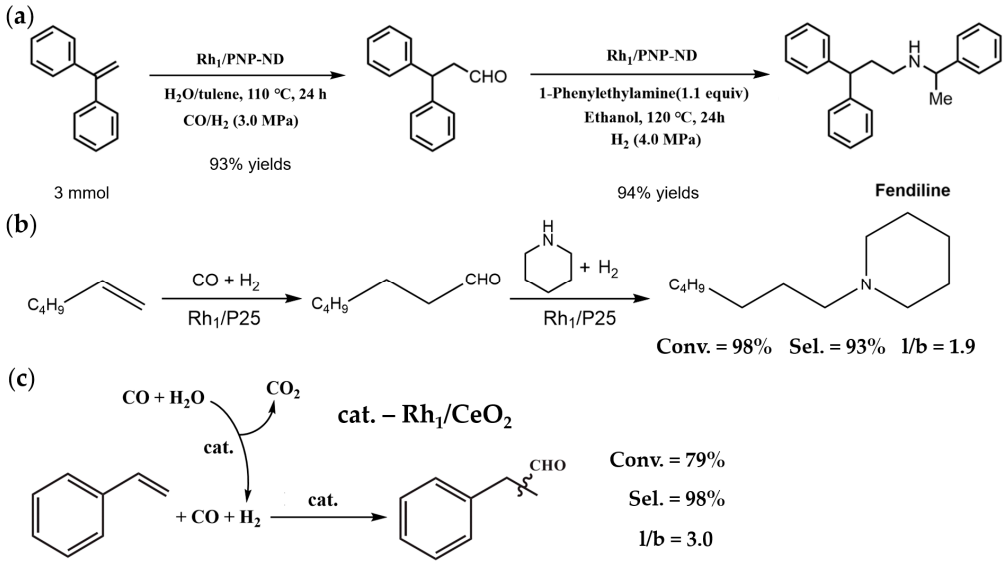


**Figure 11.** (**a**) The synthesis of fendiline with one-pot hydroformylation/amination reaction. Adapted with permission from ref. [52] Copyright 2021 Gao, P. et al. (**b**) Hydroaminoalkylation of 1-hexene. Adapted with permission from ref. [53] Copyright 2023 John Wiley and Sons. (**c**) Hydroformylation coupling with water–gas shift reaction could improve the regioselectivity of aldehyde. Adapted with permission from ref. [54] Copyright 2020 John Wiley and Sons.

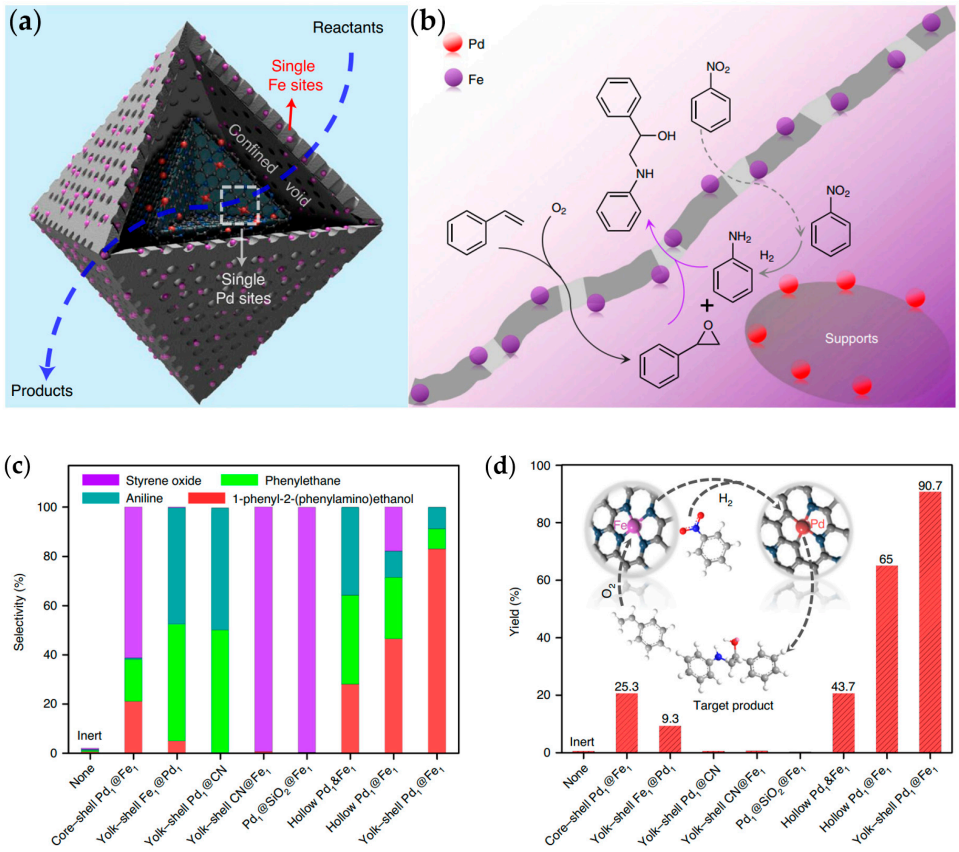


**Figure 12.** (**a**) Schematic illustration of the yolk–shell nanostructure of $Pd_1$@$Fe_1$. (**b**)The proposed reaction scheme for the epoxide ring-opening amination tandem reaction. (**c**) The selectivity of various as-prepared catalysts. (**d**) Yields of the target product(1-phenyl-2-(phenylamino)ethanol). All reproduced from ref. [56] Copyright 2021 Zhao, Y. et al.

## 4. Conclusions and Perspective

In this review, we have summarized recent advances regarding the functionalization of alkenes utilizing SACs. These catalytic transformations are not only widely used in preparing pharmaceutical intermediates, but they are also of great value in the field of material synthesis, including as aerogels and surfactants. From the above discussions, single-atom catalysis has made much progress in the field over the last decade and has gradually developed into a practical alternative approach, especially for reactions that are industrially realized with homogeneous catalysts. For example, in 2020, the first heterogeneous single-Rh-atom-catalyzed hydroformylation-hydrogenation reactions were put into operation in Ningbo, China, with an annual capacity to produce 50,000 tons of *n*-propanol from ethylene and syngas [57]. The superior reactivity and stability of Rh SACs demonstrate that single-atom catalysis can be a bridge to connect both homogeneous and heterogeneous catalysis, and more practical applications of SACs may soon appear. We also note that SACs have been applied in the photocatalytic [39] and electrocatalytic [51] conversion of alkenes, which could further meet the sustainable demand of using renewable energy to reduce traditional fossil energy consumption.

Regarding catalyst design, singly dispersed metal sites can be regarded as simplified models in heterogeneous catalysts, thus facilitating DFT predictions concerning the plausible reaction pathways on different kinds of metal centers. As a result, optimized catalytic active structures can be intentionally fabricated without repeating time-consuming test-error processes. Moreover, a basic understanding concerning single-atom catalytic sites provides valuable mechanism insight in preparing multi-metal centers with good catalytic performance, such as the yolk–shell Pd-Fe dual atoms [55] and synergetic sites involving metal clusters/NPs along with single atoms.

Despite the above achievements, single-atom catalysis faces challenges as well. For one thing, although some reaction pathways were proposed and accepted in principle, the detailed reaction mechanisms in alkene transformations are still lacking. As a result, in situ characterization techniques are needed to track the structure change in active metal species, revealing the real active state under working conditions. For another thing, the existing SAC systems could be further improved for potential industrial applications, and more effort should be spent on exploring SACs with non-noble metal centers to reduce catalyst costs. In addition, the deactivation of catalysts under harsh reaction conditions, such as reducing atmospheres and elevating temperatures, is frequently caused by the aggregation of isolated metal atoms. Therefore, the surface properties of supports should be carefully tuned to anchor single-metal atoms in high loadings. Moreover, new regeneration strategies need to be developed for recovering catalytic performance.

**Author Contributions:** Conceptualization, R.L. and B.Q.; data curation, all the authors; writing—original draft preparation, X.Y. and Y.J. (Yuxia Ji); writing—review and editing, R.L.; figures X.Y. and Y.J. (Yan Jiang); supervision, Y.F. All authors have read and agreed to the published version of the manuscript.

**Funding:** This research was funded by the Guangzhou Projects for Fundamental Research, grant number 202102020202, the Guangdong Provincial Key Laboratory of Plant Resources Biorefinery, grant number 2021GDKLPRB10, and the Start-up Funding of Guangdong University of Technology, grant numbers 220413279, 212210146 and 212200373.

**Data Availability Statement:** Not applicable.

**Conflicts of Interest:** The authors declare no conflict of interest.

## References

1. Komiyama, T.; Minami, Y.; Hiyama, T. Recent Advances in Transition-Metal-Catalyzed Synthetic Transformations of Organosilicon Reagents. *ACS Catal.* **2016**, *7*, 631–651. [CrossRef]
2. Franke, R.; Selent, D.; Borner, A. Applied hydroformylation. *Chem. Rev.* **2012**, *112*, 5675–5732. [CrossRef]
3. Troegel, D.; Stohrer, J. Recent advances and actual challenges in late transition metal catalyzed hydrosilylation of olefins from an industrial point of view. *Coord. Chem. Rev.* **2011**, *255*, 1440–1459. [CrossRef]

4. Qiao, B.; Wang, A.; Yang, X.; Allard, L.F.; Jiang, Z.; Cui, Y.; Liu, J.; Li, J.; Zhang, T. Single-atom catalysis of CO oxidation using $Pt_1/FeO_x$. *Nat. Chem.* **2011**, *3*, 634–641. [CrossRef] [PubMed]
5. Yang, X.-F.; Wang, A.; Qiao, B.; Li, J.; Liu, J.; Zhang, T. Single-Atom Catalysts: A New Frontier in Heterogeneous Catalysis. *Acc. Chem. Res.* **2013**, *46*, 1740–1748. [CrossRef]
6. Chen, Z.; Liu, J.; Koh, M.J.; Loh, K.P. Single-Atom Catalysis: From Simple Reactions to the Synthesis of Complex Molecules. *Adv. Mater.* **2022**, *34*, e2103882. [CrossRef]
7. Sakaki, S.; Mizoe, N.; Sugimoto, M.; Musashi, Y. Pt-catalyzed hydrosilylation of ethylene. A theoretical study of the reaction mechanism. *Coord. Chem. Rev.* **1999**, *190–192*, 933–960. [CrossRef]
8. Cui, X.; Junge, K.; Dai, X.; Kreyenschulte, C.; Pohl, M.M.; Wohlrab, S.; Shi, F.; Bruckner, A.; Beller, M. Synthesis of Single Atom Based Heterogeneous Platinum Catalysts: High Selectivity and Activity for Hydrosilylation Reactions. *ACS Cent. Sci.* **2017**, *3*, 580–585. [CrossRef]
9. Zhu, Y.; Cao, T.; Cao, C.; Luo, J.; Chen, W.; Zheng, L.; Dong, J.; Zhang, J.; Han, Y.; Li, Z.; et al. One-Pot Pyrolysis to N-Doped Graphene with High-Density Pt Single Atomic Sites as Heterogeneous Catalyst for Alkene Hydrosilylation. *ACS Catal.* **2018**, *8*, 10004–10011. [CrossRef]
10. Zhang, L.; Zhang, H.; Liu, K.; Hou, J.; Badamdorj, B.; Tarakina, N.V.; Wang, M.; Wang, Q.; Wang, X.; Antonietti, M. In-situ Synthesis of -P=N-doped Carbon Nanofibers for Single Atom Catalytic Hydrosilylation. *Adv. Mater.* **2023**, e2209310. [CrossRef]
11. Liu, K.; Badamdorj, B.; Yang, F.; Janik, M.J.; Antonietti, M. Accelerated Anti-Markovnikov Alkene Hydrosilylation with Humic-Acid-Supported Electron-Deficient Platinum Single Atoms. *Angew. Chem., Int. Ed.* **2021**, *60*, 24220–24226. [CrossRef] [PubMed]
12. Han, Y.; Xiong, Y.; Liu, C.; Zhang, H.; Zhao, M.; Chen, W.; Chen, W.; Huang, W. Electron-rich isolated Pt active sites in ultrafine $PtFe_3$ intermetallic catalyst for efficient alkene hydrosilylation. *J. Catal.* **2021**, *396*, 351–359. [CrossRef]
13. Pan, G.; Hu, C.; Hong, S.; Li, H.; Yu, D.; Cui, C.; Li, Q.; Liang, N.; Jiang, Y.; Zheng, L.; et al. Biomimetic caged platinum catalyst for hydrosilylation reaction with high site selectivity. *Nat. Commun.* **2021**, *12*, 64. [CrossRef] [PubMed]
14. Li, M.; Zhao, S.; Li, J.; Chen, X.; Ji, Y.; Yu, H.; Bai, D.; Xu, G.; Zhong, Z.; Su, F. Partially charged single-atom Ru supported on $ZrO_2$ nanocrystals for highly efficient ethylene hydrosilylation with triethoxysilane. *Nano Res.* **2022**, *15*, 5857–5864. [CrossRef]
15. Lee, S.; Patra, A.; Christopher, P.; Vlachos, D.G.; Caratzoulas, S. Theoretical Study of Ethylene Hydroformylation on Atomically Dispersed $Rh/Al_2O_3$ Catalysts: Reaction Mechanism and Influence of the $ReO_x$ Promoter. *ACS Catal.* **2021**, *11*, 9506–9518. [CrossRef]
16. Amsler, J.; Sarma, B.B.; Agostini, G.; Prieto, G.; Plessow, P.N.; Studt, F. Prospects of Heterogeneous Hydroformylation with Supported Single Atom Catalysts. *J. Am. Chem. Soc.* **2020**, *142*, 5087–5096. [CrossRef]
17. Farpon, M.G.; Henao, W.; Plessow, P.N.; Andres, E.; Arenal, R.; Marini, C.; Agostini, G.; Studt, F.; Prieto, G. Rhodium Single-Atom Catalyst Design through Oxide Support Modulation for Selective Gas-Phase Ethylene Hydroformylation. *Angew. Chem. Int. Ed.* **2023**, *62*, e202214048. [CrossRef]
18. Ro, I.; Qi, J.; Lee, S.; Xu, M.; Yan, X.; Xie, Z.; Zakem, G.; Morales, A.; Chen, J.G.; Pan, X.; et al. Bifunctional hydroformylation on heterogeneous Rh-$WO_x$ pair site catalysts. *Nature* **2022**, *609*, 287–292. [CrossRef]
19. Lang, R.; Li, T.; Matsumura, D.; Miao, S.; Ren, Y.; Cui, Y.T.; Tan, Y.; Qiao, B.; Li, L.; Wang, A.; et al. Hydroformylation of Olefins by a Rhodium Single-Atom Catalyst with Activity Comparable to $RhCl(PPh_3)_3$. *Angew. Chem. Int. Ed.* **2016**, *55*, 16054–16058. [CrossRef]
20. Shang, W.; Qin, B.; Gao, M.; Qin, X.; Chai, Y.; Wu, G.; Guan, N.; Ma, D.; Li, L. Efficient Heterogeneous Hydroformylation over Zeolite-Encaged Isolated Rhodium Ions. *CCS Chem.* **2022**, *in press*. [CrossRef]
21. Zhao, K.; Wang, H.; Wang, X.; Li, T.; Dai, X.; Zhang, L.; Cui, X.; Shi, F. Confinement of atomically dispersed Rh catalysts within porous monophosphine polymers for regioselective hydroformylation of alkenes. *J. Catal.* **2021**, *401*, 321–330. [CrossRef]
22. Escobar-Bedia, F.J.; Lopez-Haro, M.; Calvino, J.J.; Martin-Diaconescu, V.; Simonelli, L.; Perez-Dieste, V.; Sabater, M.J.; Concepción, P.; Corma, A. Active and Regioselective Ru Single-Site Heterogeneous Catalysts for Alpha-Olefin Hydroformylation. *ACS Catal.* **2022**, *12*, 4182–4193. [CrossRef]
23. Gong, H.; Zhao, X.; Qin, Y.; Xu, W.; Wei, X.; Peng, Q.; Ma, Y.; Dai, S.; An, P.; Hou, Z. Hydroformylation of olefins catalyzed by single-atom Co(II) sites in zirconium phosphate. *J. Catal.* **2022**, *408*, 245–260. [CrossRef]
24. Wei, B.; Chen, J.; Liu, X.; Hua, K.; Li, L.; Zhang, S.; Luo, H.; Wang, H.; Sun, Y. Achieving rhodium-like activity for olefin hydroformylation by electronic metal-support interaction of single atomic cobalt catalyst. *Cell Rep. Phys. Sci.* **2022**, *3*, 101016. [CrossRef]
25. Xu, Q.; Guo, C.; Tian, S.; Zhang, J.; Chen, W.; Cheong, W.-C.; Gu, L.; Zheng, L.; Xiao, J.; Liu, Q.; et al. Coordination structure dominated performance of single-atomic Pt catalyst for anti-Markovnikov hydroboration of alkenes. *Sci. China Mater.* **2020**, *63*, 972–981. [CrossRef]
26. Xu, Q.; Guo, C.; Li, B.; Zhang, Z.; Qiu, Y.; Tian, S.; Zheng, L.; Gu, L.; Yan, W.; Wang, D.; et al. $Al^{3+}$ Dopants Induced $Mg^{2+}$ Vacancies Stabilizing Single-Atom Cu Catalyst for Efficient Free-Radical Hydrophosphinylation of Alkenes. *J. Am. Chem. Soc.* **2022**, *144*, 4321–4326. [CrossRef] [PubMed]
27. Wen, J.; Yang, X.; Sun, Z.; Yang, J.; Han, P.; Liu, Q.; Dong, H.; Gu, M.; Huang, L.; Wang, H. Biomimetic photocatalytic sulfonation of alkenes to access $\beta$-ketosulfones with single-atom iron site. *Green Chem.* **2020**, *22*, 230–237. [CrossRef]
28. Yang, J.; Sun, Z.; Yan, K.; Dong, H.; Dong, H.; Cui, J.; Gong, X.; Han, S.; Huang, L.; Wen, J. Single-atom-nickel photocatalytic site-selective sulfonation of enamides to access amidosulfones. *Green Chem.* **2021**, *23*, 2756–2762. [CrossRef]

29. Xue, W.; Zhu, Z.; Chen, S.; You, B.; Tang, C. Atomically Dispersed Co-N/C Catalyst for Divergent Synthesis of Nitrogen-Containing Compounds from Alkenes. *J. Am. Chem. Soc.* **2023**, *145*, 4142–4149. [CrossRef]
30. Zhou, X.; Sterbinsky, G.E.; Wasim, E.; Chen, L.; Tait, S.L. Tuning Ligand-Coordinated Single Metal Atoms on $TiO_2$ and their Dynamic Response during Hydrogenation Catalysis. *ChemSusChem* **2021**, *14*, 3825–3837. [CrossRef]
31. Zhang, L.; Zhou, M.; Wang, A.; Zhang, T. Selective Hydrogenation over Supported Metal Catalysts: From Nanoparticles to Single Atoms. *Chem. Rev.* **2020**, *120*, 683–733. [CrossRef]
32. Lang, R.; Du, X.; Huang, Y.; Jiang, X.; Zhang, Q.; Guo, Y.; Liu, K.; Qiao, B.; Wang, A.; Zhang, T. Single-Atom Catalysts Based on the Metal–Oxide Interaction. *Chem. Rev.* **2020**, *120*, 11986–12043. [CrossRef]
33. Liu, L.; Corma, A. Metal Catalysts for Heterogeneous Catalysis: From Single Atoms to Nanoclusters and Nanoparticles. *Chem. Rev.* **2018**, *118*, 4981–5079. [CrossRef]
34. Mondelli, C.; Gözaydın, G.; Yan, N.; Pérez-Ramírez, J. Biomass valorisation over metal-based solid catalysts from nanoparticles to single atoms. *Chem. Soc. Rev.* **2020**, *49*, 3764–3782. [CrossRef]
35. Abdel-Mageed, A.M.; Wohlrab, S. Review of $CO_2$ Reduction on Supported Metals (Alloys) and Single-Atom Catalysts (SACs) for the Use of Green Hydrogen in Power-to-Gas Concepts. *Catalysts* **2022**, *12*, 16. [CrossRef]
36. Wang, Y.; Wang, M.; Mou, X.; Wang, S.; Jiang, X.; Chen, Z.; Jiang, Z.; Lin, R.; Ding, Y. Host-induced alteration of the neighbors of single platinum atoms enables selective and stable hydrogenation of butadiene. *Nanoscale* **2022**, *14*, 10506–10513. [CrossRef]
37. Hu, F.; Leng, L.; Zhang, M.; Chen, W.; Yu, Y.; Wang, J.; Horton, J.H.; Li, Z. Direct Synthesis of Atomically Dispersed Palladium Atoms Supported on Graphitic Carbon Nitride for Efficient Selective Hydrogenation Reactions. *ACS Appl. Mater. Interfaces* **2020**, *12*, 54146–54154. [CrossRef] [PubMed]
38. Yan, H.; Cheng, H.; Yi, H.; Lin, Y.; Yao, T.; Wang, C.; Li, J.; Wei, S.; Lu, J. Single-Atom $Pd_1$/Graphene Catalyst Achieved by Atomic Layer Deposition: Remarkable Performance in Selective Hydrogenation of 1,3-Butadiene. *J. Am. Chem. Soc.* **2015**, *137*, 10484–10487. [CrossRef]
39. Zhao, E.; Li, M.; Xu, B.; Wang, X.L.; Jing, Y.; Ma, D.; Mitchell, S.; Pérez-Ramírez, J.; Chen, Z. Transfer Hydrogenation with a Carbon-Nitride-Supported Palladium Single-Atom Photocatalyst and Water as a Proton Source. *Angew. Chem. Int. Ed.* **2022**, *61*, e202207410. [CrossRef]
40. Liu, W.; Morfin, F.; Provost, K.; Bahri, M.; Baaziz, W.; Ersen, O.; Piccolo, L.; Zlotea, C. Unveiling the Ir single atoms as selective active species for the partial hydrogenation of butadiene by operando XAS. *Nanoscale* **2022**, *14*, 7641–7649. [CrossRef] [PubMed]
41. Lucci, F.R.; Liu, J.; Marcinkowski, M.D.; Yang, M.; Allard, L.F.; Flytzani-Stephanopoulos, M.; Sykes, E.C. Selective hydrogenation of 1,3-butadiene on platinum-copper alloys at the single-atom limit. *Nat. Commun.* **2015**, *6*, 8550. [CrossRef]
42. Talib, S.H.; Yu, X.; Yu, Q.; Baskaran, S.; Li, J. Non-noble metal single-atom catalysts with phosphotungstic acid (PTA) support: A theoretical study of ethylene epoxidation. *Sci. China Mater.* **2020**, *63*, 1003–1014. [CrossRef]
43. Cao, R.; Thapa, R.; Kim, H.; Xu, X.; Gyu Kim, M.; Li, Q.; Park, N.; Liu, M.; Cho, J. Promotion of oxygen reduction by a bio-inspired tethered iron phthalocyanine carbon nanotube-based catalyst. *Nat. Commun.* **2013**, *4*, 2076. [CrossRef] [PubMed]
44. Liu, J.; Wang, H.; Ye, R.; Jian, P.; Wang, L. Promotional effect of Mn-doping on the catalytic performance of NiO sheets for the selective oxidation of styrene. *J. Colloid Interface Sci.* **2021**, *585*, 61–71. [CrossRef] [PubMed]
45. Zhang, Y.; Li, Y.-X.; Liu, L.; Han, Z.-B. Palladium nanoparticles supported on UiO-66-$NH_2$ as heterogeneous catalyst for epoxidation of styrene. *Inorg. Chem. Commun.* **2019**, *100*, 51–55. [CrossRef]
46. Jia, B.; Bai, L.; Han, Z.; Li, R.; Huangfu, J.; Li, C.; Zheng, J.; Qu, Y.; Leng, K.; Wang, Y.; et al. High-Performance Styrene Epoxidation with Vacancy-Defect Cobalt Single-Atom Catalysts. *ACS Appl. Mater. Interfaces* **2022**, *14*, 10337–10343. [CrossRef] [PubMed]
47. Chen, X.; Zou, Y.; Zhang, M.; Gou, W.; Zhang, S.; Qu, Y. Multiscale porous single-atom Co catalysts for epoxidation with $O_2$. *J. Mater. Chem. A* **2022**, *10*, 6016–6022. [CrossRef]
48. Li, Z.; Li, H.; Yuan, D.; Leng, L.; Zhang, M.; Di, M.; Horton, J.H.; Wang, J.; Sun, L.; Sun, W. Photoinduction of palladium single atoms supported on defect-containing γ-AlOOH nanoleaf for efficient trans-stilbene epoxidation. *Chem. Eng. J.* **2022**, *429*, 132149. [CrossRef]
49. Dong, X.; Wang, C.; Zhang, M.; Ji, S.; Leng, L.; Hugh Horton, J.; Dong, H.; Qiao, M.; Wang, Y.; Zhang, J.; et al. Atomically dispersed single ruthenium sites anchored on bismuth tungstate with synergistic geometric and electronic effects for epoxidation of trans-stilbene. *Chem. Eng. J.* **2023**, *454*, 139940. [CrossRef]
50. Yang, H.; Wang, X.; Liu, Q.; Huang, A.; Zhang, X.; Yu, Y.; Zhuang, Z.; Li, G.; Li, Y.; Peng, Q.; et al. Heterogeneous Iridium Single-Atom Molecular-like Catalysis for Epoxidation of Ethylene. *J. Am. Chem. Soc.* **2023**, *145*, 6658–6670. [CrossRef]
51. Chung, M.; Jin, K.; Zeng, J.S.; Ton, T.N.; Manthiram, K. Tuning Single-Atom Dopants on Manganese Oxide for Selective Electrocatalytic Cyclooctene Epoxidation. *J. Am. Chem. Soc.* **2022**, *144*, 17416–17422. [CrossRef] [PubMed]
52. Gao, P.; Liang, G.; Ru, T.; Liu, X.; Qi, H.; Wang, A.; Chen, F.E. Phosphorus coordinated Rh single-atom sites on nanodiamond as highly regioselective catalyst for hydroformylation of olefins. *Nat. Commun.* **2021**, *12*, 4698. [CrossRef] [PubMed]
53. Li, Y.; Tang, Y.; Tao, F.F. C-N Coupling through Hydroaminoalkylation on a Single-Atom Rh Heterogeneous Catalyst. *Angew. Chem. Int. Ed.* **2023**, *62*, e202214332. [CrossRef] [PubMed]
54. Li, T.; Chen, F.; Lang, R.; Wang, H.; Su, Y.; Qiao, B.; Wang, A.; Zhang, T. Styrene Hydroformylation with In Situ Hydrogen: Regioselectivity Control by Coupling with the Low-Temperature Water-Gas Shift Reaction. *Angew. Chem. Int. Ed.* **2020**, *59*, 7430–7434. [CrossRef]

55. Sarma, B.B.; Kim, J.; Amsler, J.; Agostini, G.; Weidenthaler, C.; Pfander, N.; Arenal, R.; Concepcion, P.; Plessow, P.; Studt, F.; et al. One-Pot Cooperation of Single-Atom Rh and Ru Solid Catalysts for a Selective Tandem Olefin Isomerization-Hydrosilylation Process. *Angew. Chem. Int. Ed.* **2020**, *59*, 5806–5815. [CrossRef]
56. Zhao, Y.; Zhou, H.; Zhu, X.; Qu, Y.; Xiong, C.; Xue, Z.; Zhang, Q.; Liu, X.; Zhou, F.; Mou, X.; et al. Simultaneous oxidative and reductive reactions in one system by atomic design. *Nat. Catal.* **2021**, *4*, 134–143. [CrossRef]
57. Zhou, Y.; Jiang, Y.; Ji, Y.; Lang, R.; Fang, Y.; Wu, C.D. The Opportunities and Challenges in Single-Atom Catalysis. *ChemCatChem* **2023**, *15*, e202201176. [CrossRef]